OPAL Physics Note PN293
21^{st} May 1997

A study of energy flows based on jet classification in deep inelastic electron-photon scattering

The OPAL Collaboration

Abstract

It has already been shown that the hadronic energy flow distributions in deep inelastic electron photon scattering processes disagree with those predicted by QCD models, generating serious systematic errors in the unfolding of the photon structure function F_2^γ. The analysis presented here uses a jet classification of the hadronic final state based on the cone jet finder to identify the class of events which is in worst agreement with the models, in the medium Q^2 region of $6 \leq Q^2 \leq 30$ GeV^2. In addition to the QCD-based Monte Carlo models, HERWIG and PYTHIA, the simple F2GEN program is used for comparisons with the data which was taken at e^+e^-centre-of-mass energies close to the Z^0mass.

This note describes preliminary OPAL results to be submitted to the XVIII International Symposium on Lepton-Photon Interactions, Hamburg, 28 July - 1 August 1997, and to the International Europhysics Conference on High Energy Physics, Jerusalem, 19-26 August 1997

1 Introduction

In the singly-tagged regime, the process $e^+e^- \to e^+e^- +$ hadrons can be regarded as deep inelastic scattering of an $e^\pm$ on a quasi-real photon. The flux of quasi-real photons can be calculated using the equivalent photon approximation [1, 2]. Figure 1 shows a diagram of this reaction. The four-vector of the incoming electron which radiates the virtual photon is denoted k. This electron scatters into the detector at an angle $\theta_{\rm tag}$ to the beam and with an energy $E_{\rm tag}$. The four-vectors of the virtual photon and the quasi-real photon are represented by q and p, respectively. The symbol $\mathrm{f}_{\mathrm{q},\gamma}(\mathrm{x}, Q^2)$ represents the parton densities of the quasi-real photon. $Q^2 = -q^2$ is the negative value of the four-momentum squared of the virtual photon. W is the invariant mass of the $\gamma^\star\gamma$ system and is calculated using the measured four-momenta of the hadronic final state particles.

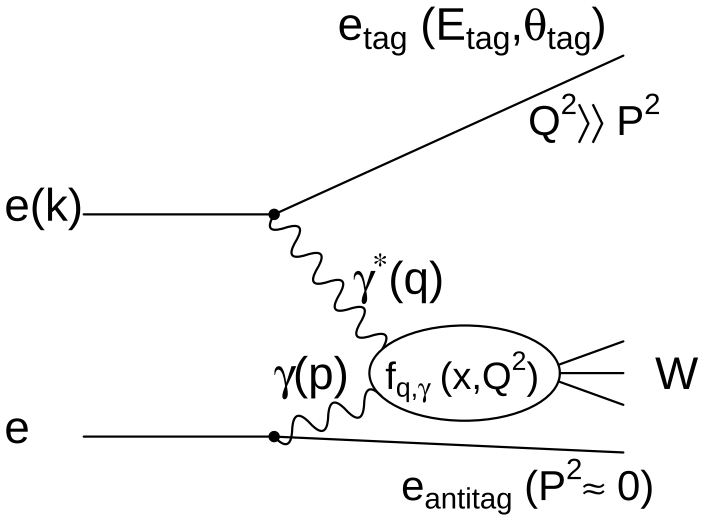

Figure 1: A diagram of deep inelastic $e\gamma$ scattering.

In contrast to deep inelastic charged lepton-nucleon scattering, where the energies of both interacting particles are given, in deep inelastic electron-photon reactions the energy of the incoming quasi-real photon is not known. As a consequence of this, the kinematics of the reaction in terms of x and Q^2 are not fully determined by measuring the four-vector of the tagged electron. The value of x has to be obtained by measuring the hadronic final state, which is only partly observed in the detector. This leads to the dependence of F_2^γ on the modelling of the hadronic final state by the Monte Carlo programs which are used for unfolding.

A previous OPAL paper [3] has shown that there are currently problems in extracting the photon structure function F_2^γ from deep inelastic electron-photon scattering events at LEP. None of the available models gives a good representation of the hadronic energy flow in the data in the central region and forward regions of the detector, and especially for low values of $x_{\rm vis}$, the visible x. This study attempts to characterize the observed discrepancies by the number of hadronic jets reconstructed in the laboratory frame. Measurments and model predictions of the energy flow distributions are compared for classes of events with 0, 1 or 2 jets.

2 The OPAL detector

The OPAL detector is described in detail elsewhere [4]; only the subdetectors which are most relevant for this analysis, namely the electromagnetic calorimeters and the tracking devices, are detailed below[1]. There is a uniform magnetic field of 0.435 T along the beam direction throughout the central tracking region, with electromagnetic and hadronic calorimetry and muon chambers outside the coil.

The forward detectors (FD) cover the acceptance region in θ from 60 to 140 mrad at each end of the OPAL detector. They consist of cylindrical lead-scintillator calorimeters with a depth of 24 radiation lengths (X_0) divided azimuthally into 16 segments. The energy resolution for electromagnetic showers is $18\%/\sqrt{E}$, where E is in GeV. An array of three planes of proportional tubes buried in the calorimeter at a depth of 4 X_0 provides a precise shower position measurement, with a typical resolution of 3–4 mm, corresponding to 2.5 mrad in θ, and less than 3.5 mrad in ϕ. A small-angle silicon tungsten luminometer (SW) extends the acceptance region in θ down to 25 mrad. The space between the outer edge of the FD and the inner edge of the electromagnetic endcap calorimeter is filled by a small annular lead-scintillator calorimeter, the gamma catcher.

The endcap electromagnetic calorimeters are homogeneous devices composed of arrays of lead-glass blocks of 9.2×9.2 cm^2 cross-section and typically 22 X_0 in depth, giving good shower containment. The endcaps cover the angular range from 200 to 630 mrad. The energy resolution is typically $15\%/\sqrt{E}$, where E is in GeV, at angles above 350 mrad, but becomes worse closer to the edge of the detector.

Charged particles are detected by a silicon microvertex detector, a drift chamber vertex detector, and a jet chamber. Outside the jet chamber, but still in the magnetic field, lies a layer of drift chambers whose purpose is to improve the track reconstruction in the z-coordinate parallel to the beam direction. The resolution of the transverse momentum for charged particles is $\frac{\sigma_{p_{\rm t}}}{p_{\rm t}} = \sqrt{0.02^2 + (0.0015\, p_{\rm t})^2}$ for $|\cos\theta| < 0.7$ and degrades for higher values of $|\cos\theta|$. Outside the solenoid is the electromagnetic barrel calorimeter, of similar construction to the endcaps described above.

[1] In the OPAL right-handed coordinate system the x-axis points towards the centre of the LEP ring, the y-axis points upwards and the z-axis points in the direction of the electron beam. The polar angle θ and the azimuthal angle ϕ are defined with respect to the z-axis and x-axis, respectively.

3 Data selection, background simulation and jet reconstruction

The analysis uses the data from the 1994 and 1995 LEP runs, with e^+e^- centre-of-mass energies close to the Z^0 mass. The total integrated e^+e^- luminosity, determined from small-angle Bhabha scattering events, is 79.4 ± 0.2 pb^{-1}. The tagged electron is detected in the forward detectors ($Q^2 \approx 6-30\,\mathrm{GeV}^2$). Candidate events for the process $e\gamma \to$ hadrons are required to satisfy criteria for the tagged electron as well as for the hadronic final state, in addition to several technical cuts to ensure good detector status and track quality. The event selection listed below corresponds to the low Q^2 selection in [3]. It is designed to have a high efficiency for signal events and to reject background events.

1. A tagged electron candidate is required which produces a cluster in a forward detector with energy $E_{\mathrm{tag}} \geq 0.775\,E_{\mathrm{b}}$ and polar angle $60 \leq \theta_{\mathrm{tag}} \leq 120$ mrad with respect to either of the beam directions. E_{b} is the beam energy.
2. The energy E_{a} of the most energetic cluster in the hemisphere opposite to the one which contains the tagged electron is restricted to $E_{\mathrm{a}} \leq 0.25\,E_{\mathrm{b}}$ (antitag requirement).
3. At least three good tracks originating from the hadronic final state have to be present.
4. The visible invariant mass $W_{\mathrm{vis}} = \sqrt{E^2_{\mathrm{vis}} - p^2_{\mathrm{vis}}}$ of the hadronic system is required to be in the range $2.5 \leq W_{\mathrm{vis}} \leq 40$ GeV. E_{vis} and p_{vis} are the sums of the energies and momenta respectively of the hadronic final state particles.

Version 1.51 of the MT [5] algorithm is used with default settings to perform quality cuts on tracks and calorimeter clusters and to match clusters with tracks. A particle is defined to be an object whose 4-momentum vector is an output of the algorithm. 2720 data events survive the cuts.

The dominant background sources are $\gamma^\star\gamma \to \tau^+\tau^-$and $Z^0 \to$ hadrons. They are simulated with the Vermaseren program [6] and with the JETSET [7, 8] Monte Carlo respectively. After normalising to the data luminosity, 147.2 ± 6.5 $\gamma^\star\gamma \to \tau^+\tau^-$ and 57.1 ± 5.2 $Z^0 \to$ hadrons events are expected to pass the event selection cuts.

Additional background sources are four-fermion events with $e^+e^-\,q\bar{q}$ and $e^+e^-\,\tau^+\tau^-$ final states, and $Z^0 \to \tau^+\tau^-$ events. The four-fermion events from the annihilation, bremsstrahlung and conversion diagrams (see Ref. [9] for details) have been simulated by the FERMISV [10] and PYTHIA programs, and the $Z^0 \to \tau^+\tau^-$ events by the KORALZ generator [11]. The contributions from these additional background sources is less than 0.5%. The total of all background events is approximately 8% (table 1). Using sets of independent triggers, the trigger efficiency is evaluated to be 99.6%.

The same cone jet finding algorithm is used to analyse tagged electron-photon events as was used in reference [12] to study untagged $\gamma\gamma$ events in OPAL. A full description of the steps in the algorithm can be found in [13]. A jet is defined as the set of particles contained in a cone of size R,

$$R = \sqrt{(\Delta\eta)^2 + (\Delta\phi)^2}, \tag{1}$$

with the cone axis defined by the direction of the momentum sum of the constituent particles. $\Delta\eta$ and $\Delta\phi$ are the differences in the pseudorapidity and the azimuthal angle between the cone axis and the particle direction.

In the algorithm, the i^{th} particle's values of η_{i}, ϕ_{i}, and transverse energy, $E_{\mathrm{T_i}} = E_{\mathrm{i}}|\sin\theta_{\mathrm{i}}|$, relative to the z-axis are used to define an initial axis and transverse energy for making a jet candidate. The candidate is constructed by iterating over the particles contained inside a cone of size $R = 1$ about the initial axis to form a new transverse energy and jet axis at each iteration:

$$\begin{aligned}
\eta^{\mathrm{jet}}_{\mathrm{new}} &= \eta^{\mathrm{jet}}_{\mathrm{old}} + \frac{E_{\mathrm{T_i}}(\eta_{\mathrm{i}} - \eta^{\mathrm{jet}}_{\mathrm{old}})}{E_{\mathrm{T_i}} + E^{\mathrm{jet}}_{\mathrm{T_{old}}}} \\
\phi^{\mathrm{jet}}_{\mathrm{new}} &= \phi^{\mathrm{jet}}_{\mathrm{old}} + \frac{E_{\mathrm{T_i}}(\phi_{\mathrm{i}} - \phi^{\mathrm{jet}}_{\mathrm{old}})}{E_{\mathrm{T_i}} + E^{\mathrm{jet}}_{\mathrm{T_{old}}}} \\
E^{\mathrm{jet}}_{\mathrm{T_{new}}} &= E_{\mathrm{T_i}} + E^{\mathrm{jet}}_{\mathrm{T_{old}}}
\end{aligned} \tag{2}$$

Two candidate jets are combined if their axes lie within a cone of size R of each other. Any particle assigned to more than one jet is placed in the closest one in η and ϕ, and its contribution to the η^{jet}, ϕ^{jet} and transverse energy of the other jet(s) is removed. Jets are accepted by requiring a minimum transverse energy $E^{\mathrm{jet}}_{\mathrm{T}} = 3.0$ GeV and requiring the pseudorapidity of the jet to be within the central tracking detectors, $|\eta^{jet}| < 2$. These are the same cuts as are used in the latest OPAL study of jets in untagged events [14].

4 Monte Carlo generation

Three Monte Carlo generators are used to simulate signal events. All Monte Carlo events are passed through the OPAL detector simulation program [15] and the same reconstruction and analysis chain as the real data events.

As well as the two general purpose QCD-based generators HERWIG 5.8d [16, 17] and PYTHIA 5.718 [7, 18] the generator F2GEN, which was developed from the TWOGEN program [19] for previous OPAL analyses [20], is used for comparisons with the data. HERWIG and PYTHIA differ in the way they generate final state hadrons. They are both based on QCD-inspired models of hard parton emission followed by hadronisation. HERWIG uses the cluster model of hadronisation and PYTHIA uses the string model as implemented in JETSET. In PYTHIA, events are classified as originating from the vector meson dominance (VMD) model of the hadronic part of the photon, or as events stemming from the anomalous coupling of the photon to quarks. No equivalent separation is made in the HERWIG sample.

F2GEN generates a two-quark state in the $\gamma^{\star}\gamma$ centre-of-mass system and uses the JETSET string fragmentation algorithm to convert it to hadrons. The angular distribution of the two outgoing quarks in the $\gamma^{\star}\gamma$ centre-of-mass system is chosen to be "pointlike", which means that the distribution is the same as it would be for lepton pair production from two real photons, as if no hard final state QCD radiation occurred and as if photons had no hadron-like component – clearly an unphysically extreme case, but interesting for comparison with other models.

5 Comparison of data with Monte Carlo predictions

In this section and the next, the term data is used to describe the sample of data events for which the estimated background has been subtracted. Table 1 and figure 2 show the number of events with 0, 1, 2 and 3 jets found for the data and Monte Carlo samples using the four-momenta of the final state particles, excluding the tag. As seen in [3], the total cross-sections in all the Monte Carlo generators fall 6–15% below the data. There is a marked difference between the data and the Monte Carlo samples in the number of events with 2 jets even after allowing for the differences in total cross-sections. The number of data events with 2 jets exceeds the predicted numbers from both HERWIG and PYTHIA, but is less than in the all pointlike F2GEN sample.

Figure 3 shows the effects of varying the cone size, R, the minimum jet transverse energy, $E_{\mathrm{T}}^{\mathrm{jet}}$, and the maximum allowed absolute value of jet pseudorapidity, $|\eta_{\mathrm{jet}}|$, on the ratio of the number of 2 jet events found in a sample to the number of 2 jet events in the data sample. In each case the HERWIG and PYTHIA distributions lie systematically below the data whilst the F2GEN distributions lie systematically above the data. The ratios show small sensitivity to variations of the maximum absolute value of the jet pseudorapidity, $|\eta_{\mathrm{jet}}|$, and moderate sensitivity to variations of the cone radius, R, but vary strongly with the minimum jet transverse energy, $E_{\mathrm{T}}^{\mathrm{jet}}$, particularly for PYTHIA.

Figure 4 shows the average energy flow per event as a function of pseudorapidity, for all events and for those that have 0, 1 or 2 jets. For a sample of N events, the average energy flow per pseudorapidity bin $d\eta$ is $\frac{1}{N}\frac{dE}{d\eta}$, where E is the sum of the energies of all particles in that bin. The tagged electron is not included but was defined to be at negative η. The errors on the data points are the average energy per particle in a bin multiplied by the square root of the number of particles in that bin divided by the number of sample events. The differences between data and Monte Carlo samples seen in the distributions for all events (Fig. 4a) have already been reported [3] and are the basis for the statement in the introduction that none of the available models gives a good representation of the hadronic energy flow. The distributions in figures 4a), b) and c) show an excess of data over HERWIG and PYTHIA in the $0.9 < \eta < 1.8$ region. This excess is particularly high in the distribution for 1 jet events where all of the Monte Carlo samples lie below the data. HERWIG predicts more energy flow into the $\eta > 2.7$ region than is seen in the data for events with 0 or 1 jet. While underestimating the total number of 2 jet events, HERWIG reproduces the energy flow distributions of 2 jet events (Fig. 4d) relatively well but PYTHIA appears to be displaced to higher η. F2GEN generates too much energy in the central detector region.

In table 2 and figure 5, the contributions from the VMD and anomalous components as generated by the PYTHIA Monte Carlo are compared. There are roughly equal numbers of events generated by the VMD and anomalous processes, but the latter process produces more 2 jet events. For the 0 jet events (Fig. 5a) the anomalous events tend to reproduce the shape of the energy flow somewhat better than the VMD type events. For the 1 jet events particularly (Fig. 5b), the shape of the anomalous part is peaked in the same region as the data whilst the shape of the VMD part is flat. The shape of the energy flow of 2 jet events is reproduced relatively well by events from either process but displaced to higher η than the data.

Figure 6 shows the number of events as a function of the energy out of the tag plane, $E_{\rm t,out}$, for the whole sample as well as for events with 0, 1 and 2 jets. Here, $E_{\rm t,out} = \sum_{particles} E_i |\sin(\lambda_i)|$ where λ_i is the angle between the particle and the plane formed by the beam direction and the tagged electron. In order to directly compare the shapes of the distributions, the total samples in figure 6a) are normalised to the total number of data events, and the 0 jet, 1 jet and 2 jet sub-samples (Fig. 6b-d) are normalised to the number of data events with 0, 1 and 2 jets respectively. The differences between data and Monte Carlo samples in the distributions for all events (Fig. 6a) were also reported in the previous OPAL paper [3]. The difference for $E_{\rm t,out}$ between the data and the HERWIG and PYTHIA in figure 6a) is correlated to the underestimation of the number of jets in the data, whilst the F2GEN sample lies above the data due to its overestimation of the number of 2 jets. HERWIG and F2GEN model the transverse energy, $E_{\rm t,out}$, rather well for all event classes (Fig. 6a–c), while PYTHIA does not generate enough out-of-plane transverse energy for the 2 jet events.

Figure 7 shows the jet transverse energy distributions, $E_{\rm T}^{\rm jet}$, for events with 1 jet and events with 2 jets. The distributions for events with 1 jet (Fig. 7a) and events with 2 jets (Fig. 7b) are normalised to the number of data events with 1 jet and with 2 jets respectively. All of the Monte Carlo samples agree reasonably well with 1 jet distributions (Fig. 7a). Apart from underestimating the 2 jet rate, PYTHIA also provides too little transverse energy for these jets (Fig. 7b).

6 Conclusions

It is clear that by selecting events with two identified hadron jets of cone size $R = 1$ in the laboratory frame we have found a sub-set of the data in which the disagreements with the Monte Carlo samples are greatly enhanced, although the properties of the hadronic final state in this sub-set are reasonably well modelled by HERWIG. While the F2GEN sample, generated using the pointlike approximation, overestimates the 2 jet rate by a factor of 2.4, HERWIG and PYTHIA are too low by factors of 2.4 and 3.6 respectively. The discrepancies observed in figures 4a) and 6a) reported on in [3] originate from the disagreement in the jet rates, as well as from the imperfect description of the hadronic energy flow within the different jet classes.

All the Monte Carlo energy flow distributions lie below the data for the pseudo-rapidity region $0.9 < \eta < 1.8$ for events with 0 and 1 jet. HERWIG overestimates the energy flow into the forward region opposite the tag for events with 0 or 1 jet. F2GEN produces too much energy in the central detector for events with 2 jets. All of the Monte Carlo samples model well the $E_{\mathrm{t,out}}$ distributions for events with 1 jet, but PYTHIA underestimates the $E_{\mathrm{t,out}}$ of the events with 2 jets.

The jet classification calculated in the lab frame is a sensitive probe of the differences in the description of the hadronic final states by the different Monte Carlo models, both for the rate and the hadronic energy flow. The correlation between the jet number and the $E_{\mathrm{t,out}}$ distributions may indicate that the Monte Carlo models HERWIG and to a greater extent PYTHIA generally underestimate the transverse energy distribution of the hadronic final state and therefore jet finding will be a useful tool to improve the description of deep inelastic electron-photon scattering.

References

[1] C. F. von Weizsäcker, Z. Phys. **88** (1934) 612;
E. J. Williams, Phys. Rev. **45** (1934) 729.

[2] V. M. Budnev *et al.*, Phys. Rep. **15** (1975) 181.

[3] OPAL Collaboration, K. Ackerstaff *et al.*, Z. Phys. **C74** (1997) 33.

[4] OPAL Collaboration, K. Ahmet *et al.*, Nucl. Instr. and Meth. **A305** (1991) 275;
P. P. Allport *et al.*, Nucl. Instr. and Meth. **A324** (1993) 34;
P. P. Allport *et al.*, Nucl. Instr. and Meth. **A346** (1994) 476;
B. E. Anderson *et al.*, IEEE Transactions on Nuclear Science **41** (1994) 845.

[5] T. Omori, S. Asai, I. Nakamura and S. Yamashita, OPAL Technical Note **TN381**.

[6] J. A. M. Vermaseren, Nucl. Phys. **B229** (1983) 347;
R. Bhattacharya, G. Grammer Jr. and J. Smith, Phys. Rev. **D15** (1977) 3267;

J. Smith, J. A. M. Vermaseren and G. Grammer Jr., Phys. Rev. **D15** (1977) 3280;
J. A. M. Vermaseren, J. Smith and G. Grammer Jr., Phys. Rev. **D19** (1979) 137.

[7] T. Sjöstrand, Comp. Phys. Comm. **82** (1994) 74;
T. Sjöstrand, PYTHIA 5.7 and JETSET 7.4: Physics and Manual, CERN-TH/93-7112.

[8] T. Sjöstrand, Comp. Phys. Comm. **39** (1986) 347;
T. Sjöstrand and M. Bengtsson, Comp. Phys. Comm. **43** (1987) 367;
T. Sjöstrand, Comp. Phys. Comm. **82** (1994) 74.

[9] OPAL Collaboration, G. Alexander *et al.*, Phys. Lett. **B376** (1996) 315.

[10] J. Hilgart, R. Kleiss and F. Le Diberder, Comp. Phys. Comm. **75** (1993) 191.

[11] KORALZ 4.0 Monte Carlo, S. Jadach, B. F. L. Ward and Z. Wąs, Comp. Phys. Comm. **79** (1994) 503.

[12] OPAL Collaboration, K. Ackerstaff *et al.*, Z. Phys. **C73** (1997) 433.

[13] OPAL Collaboration, R. Akers *et al.*, Z. Phys. **C63** (1994) 197.

[14] R. Bürgin, J. Patt, S. Söldner-Rembold, OPAL Physics Note XX.

[15] J. Allison *et al.*, Nucl. Instr. and Meth. **A317** (1992) 47.

[16] G. Marchesini and B. R. Webber, Nucl. Phys. **B310** (1988) 461;
I. G. Knowles, Nucl. Phys. **B310** (1988) 571;
S. Catani, G. Marchesini and B .R. Webber, Nucl. Phys. **B349** (1991) 635;
G. Abbiendi and L. Stanco, Comp. Phys. Comm. **66** (1991) 16;
G. Abbiendi and L. Stanco, Z. Phys. **C51** (1991) 81;
M. H. Seymour, Z. Phys. **C56** (1992) 161.

[17] M. H. Seymour in L. Lönnblad *et al.*, CERN 96-01 Physics at LEP2, edited by G. Altarelli, T. Sjöstrand and F. Zwirner, (1996) Vol. 2, p. 213;
M. H. Seymour, Proceedings of the Workshop on Two-Photon Physics at LEP and HERA, Lund, May 26-28 1994, edited by G. Jarlskog and L. Jönsson, Lund University, (1994) p. 215.

[18] T. Sjöstrand in L. Lönnblad *et al.*, CERN 96-01 Physics at LEP2, edited by G. Altarelli, T. Sjöstrand and F. Zwirner, (1996) Vol. 2, p. 218.

[19] A. Buijs, W. G. J. Langeveld, M. H. Lehto and D. J. Miller, Comp. Phys. Comm. **79** (1994) 523.

[20] OPAL Collaboration, R. Akers *et al.*, Z. Phys. **C61** (1994) 199.

Sample	All Events N	0 jet N_0	1 jet N_1	2 jet N_2	3-jet N_3
Data	2720±52	852±29	1697±41	165±13	6± 2
Background Est.:					
$\gamma^\star\gamma \to \tau^+\tau^-$	147± 7	60± 4	77± 5	11± 2	–
$Z^0 \to$ hadrons	57± 5	20± 3	16± 3	19± 3	3± 1
Data - background	2516±53	773±30	1605±42	135±13	3± 3
HERWIG	2288±32	777±19	1455±25	55± 5	1± 1
PYTHIA	2154±27	706±16	1411±22	37± 4	–
F2GEN	2363±30	596±15	1435±24	332±11	0.4±0.4

Table 1: The numbers of events with 0, 1, 2 or 3 jets found for data and Monte Carlo samples. The errors given are statistical and all Monte Carlo samples are normalised to the data luminosity.

PYTHIA Component	All Events N	0 jet N_0	1 jet N_1	2 jet N_2
VMD	1007±19	361±11	634±15	11±2
Anomalous	1147±20	345±11	776±16	26±3

Table 2: The numbers of events with 0, 1 or 2 jets jets for the VMD and anomalous components of the PYTHIA generator. The errors given are statistical and the number of events are normalised to the data luminosity.

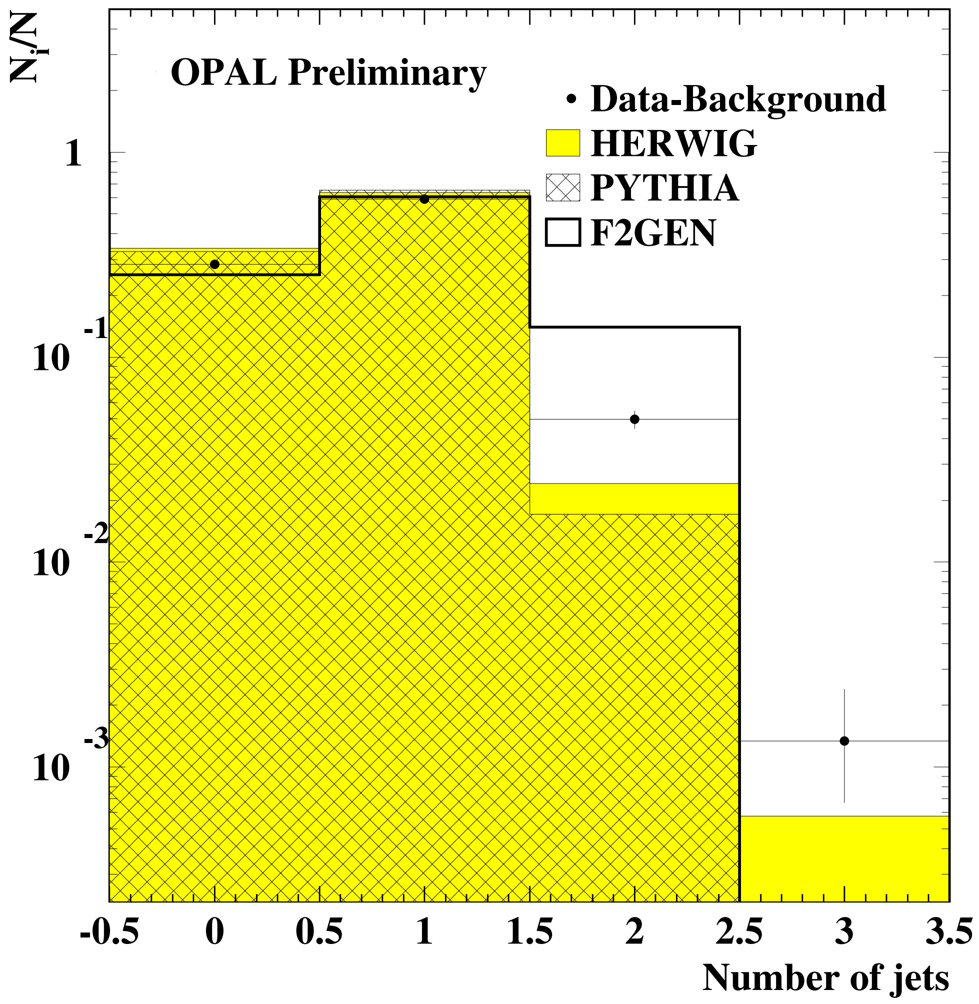

Figure 2: Fractions of events with 0–3 jets found using the measured four-momenta of the hadronic final state particles. The points show data with background subtracted, with statistical errors, and the histograms are HERWIG (shaded), PYTHIA (hatched) and F2GEN (open).

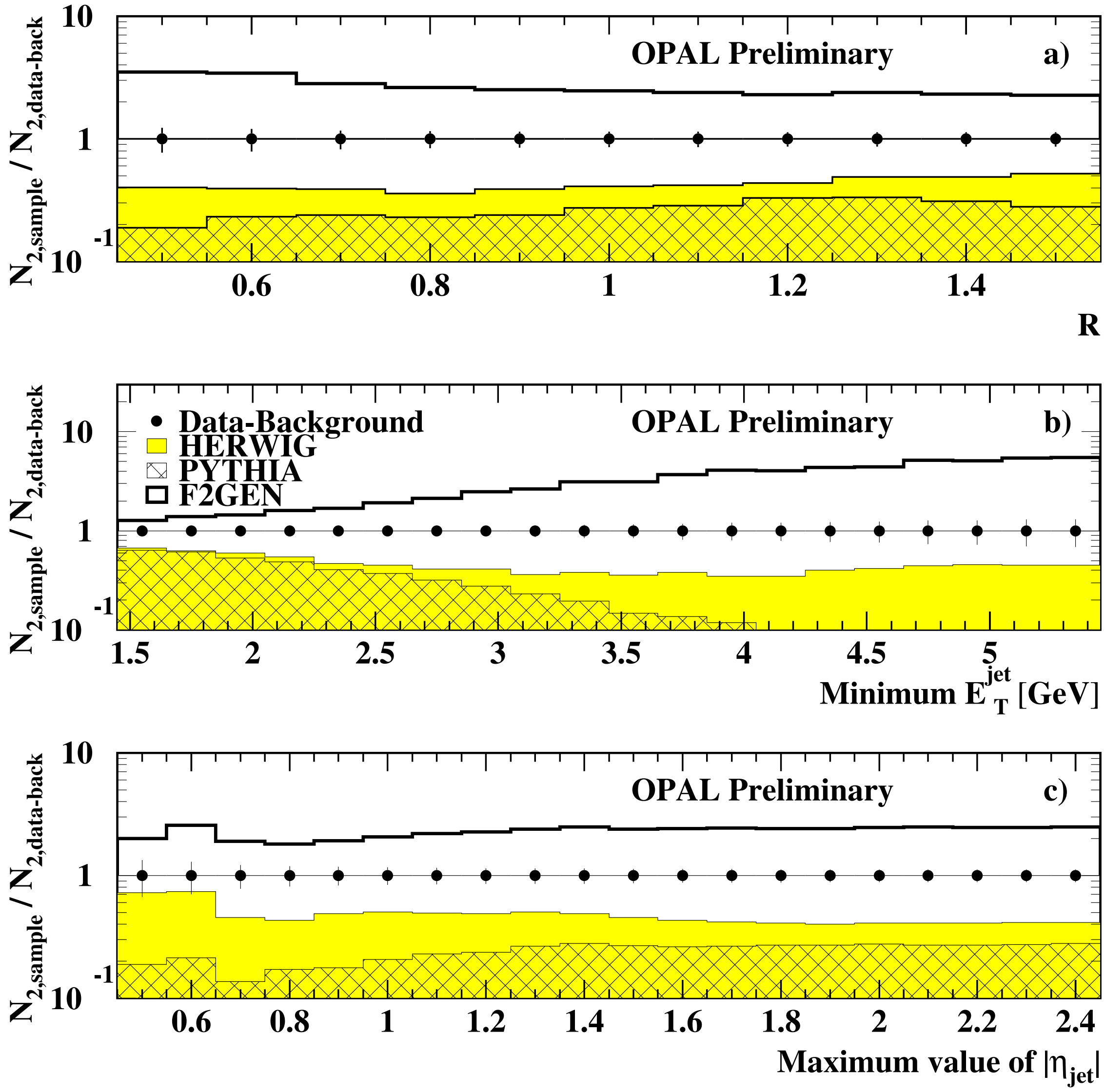

Figure 3: Ratio of the number of 2 jet events in a sample to the number of 2 jet events in the data-background sample as a function of cone size, R, in a), of minimum jet transverse energy, E_T^{jet}, in b), and of maximum allowed absolute value of jet pseudo-rapidity, $|\eta_{\rm jet}|$, in c). The samples are represented as in figure 2 and the errors in the data-background sample are purely statistical.

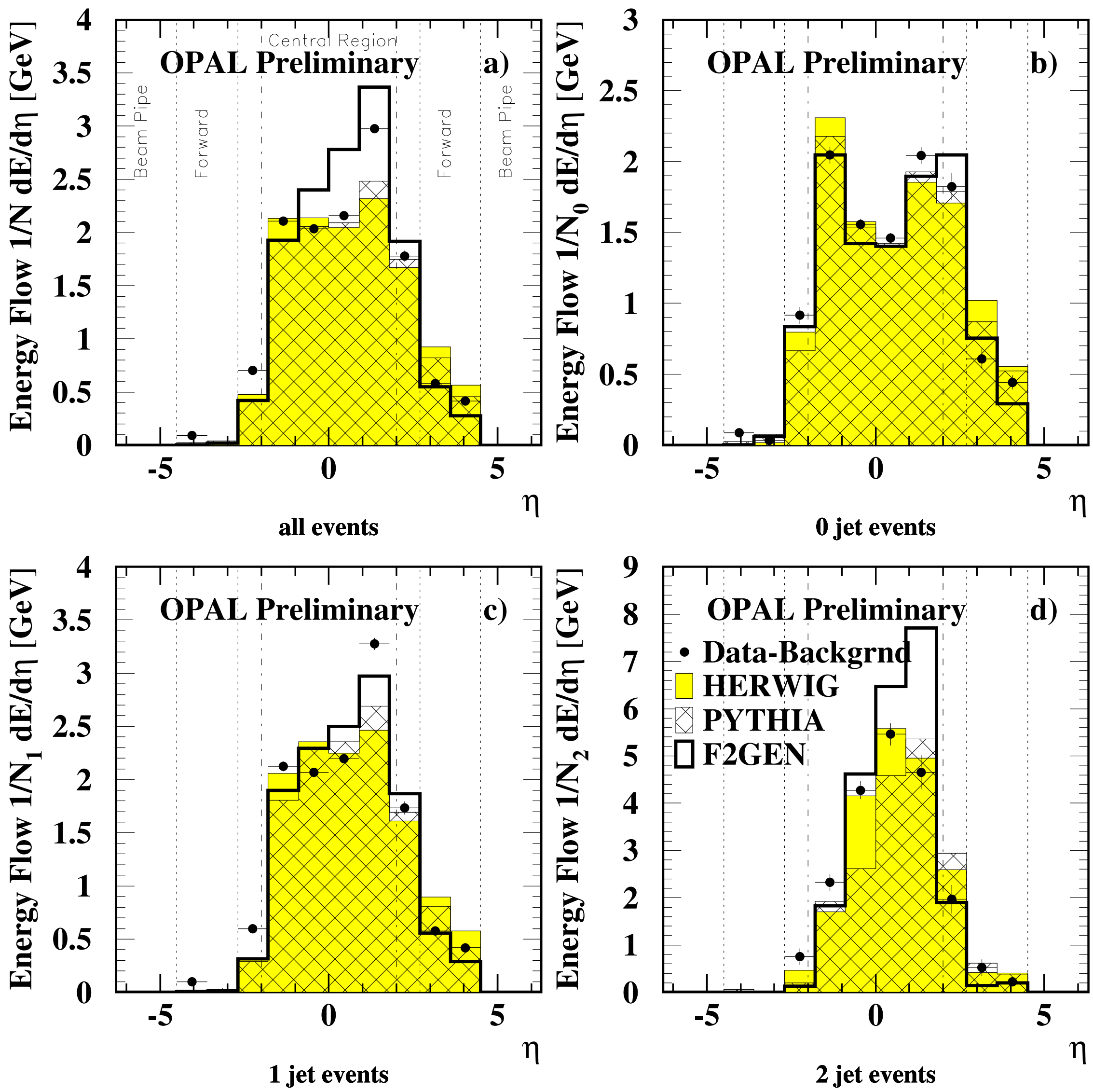

Figure 4: The hadronic energy flow per event in bins of pseudorapidity $\eta = -\ln\tan\theta'/2$. The polar angle, θ', is recalculated for all hadrons relative to the beam axis, such that the tagged electron is always at $\eta < 0$. Plot a) shows the average energy flow per event, whilst plots b), c) and d) show the same quantity for the events with 0, 1 and 2 jets respectively. The samples are represented as in figure 2, with the errors in the data-background sample calculated as described in section 5. The dotted lines show the regions of the detector in which the energy flow was measured, and the dot-dashed lines show the region of the acceptance of jets.

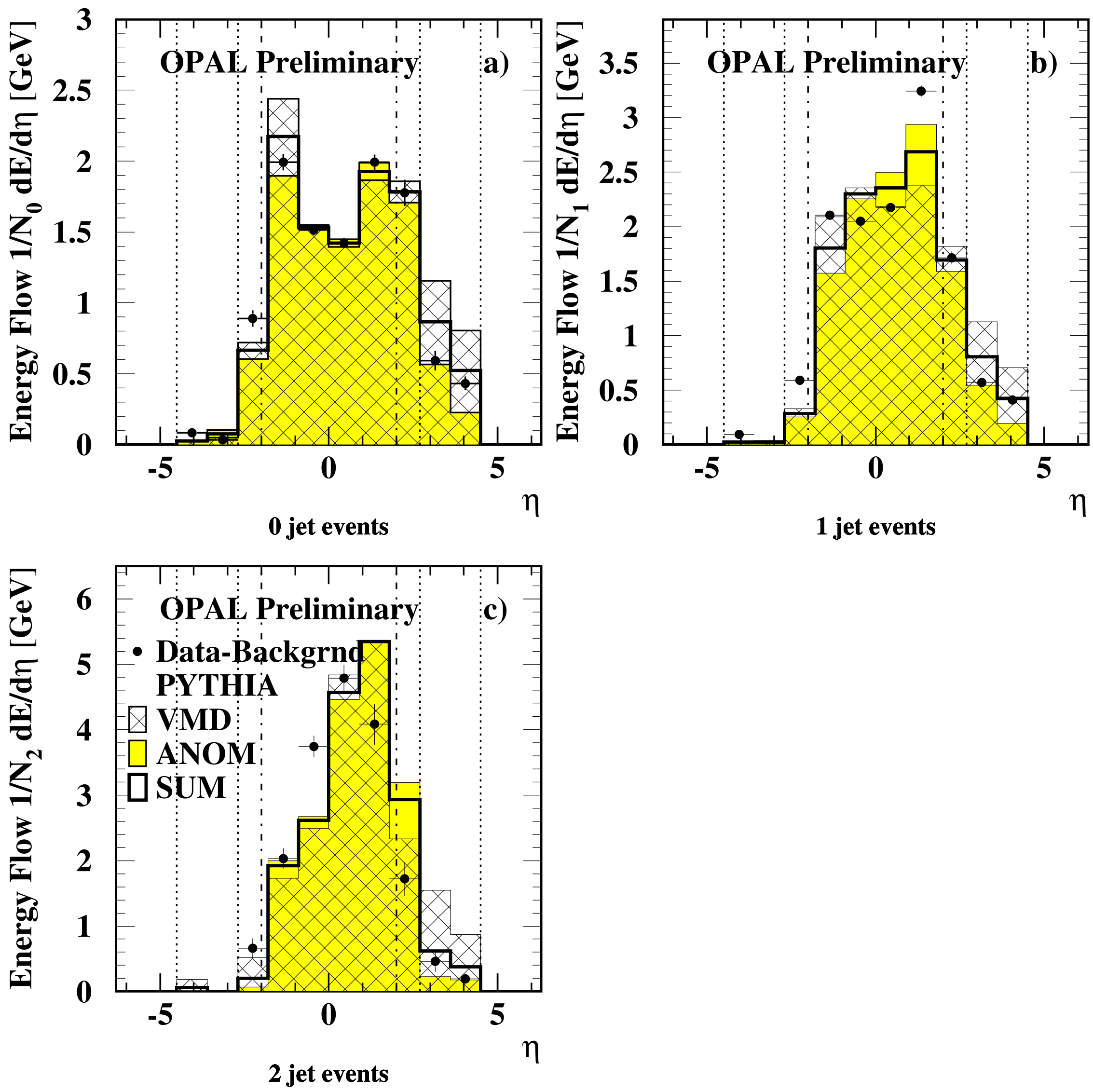

Figure 5: The average hadronic energy flow per event in bins of pseudorapidity $\eta = -\ln\tan\theta'/2$. The polar angle, θ', is recalculated for all hadrons relative to the beam axis, such that the tagged electron is always at $\eta < 0$. Plots a), b) and c) show the average hadronic energy flow for events with 0, 1 and 2 jets respectively. The points are data-background with the errors calculated as explained in section 5, and the histograms represent the PYTHIA Monte Carlo sample. The hatched and shaded histograms show the energy flows from the events generated by the VMD and anomalous components as implemented in PYTHIA and the open histograms show the combination of these in the full PYTHIA sample.

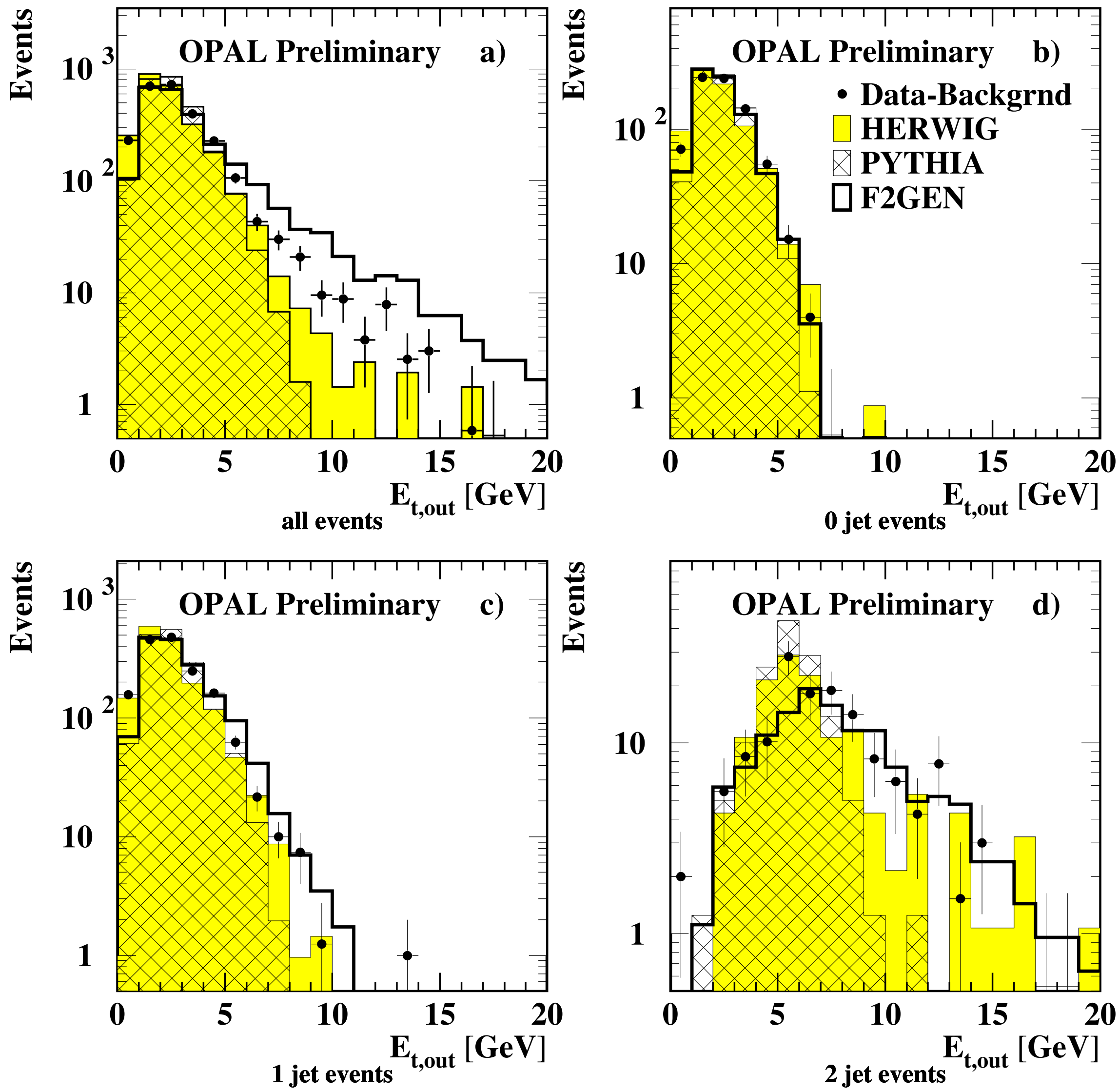

Figure 6: The transverse energy out of the plane formed by the tagged electron and the electron beams, $E_{\mathrm{t,out}}$. For the data-background, plot a), b), c) and d) show the numbers of events for the total sample and for the 0 jet, the 1 jet and the 2 jet sub-samples respectively. The Monte Carlo distributions are normalised to the same area as the data-background distributions. The samples are represented as in figure 2 and the errors in the data-background sample are purely statistical. Only entries above 0.5 are shown.

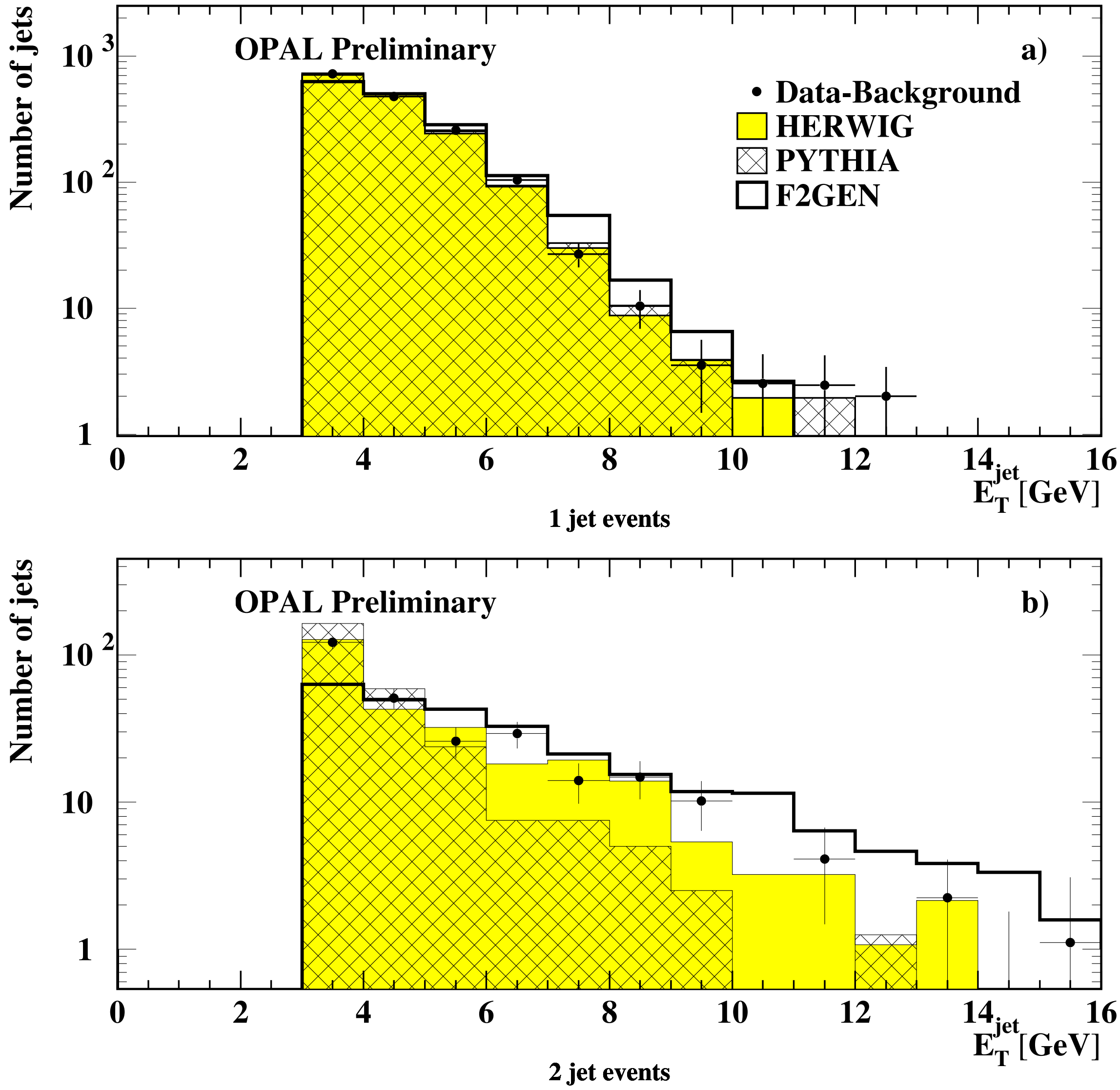

Figure 7: The jet transverse energy, $E_{\mathrm{T}}^{\mathrm{jet}}$, for a) events with 1 jet and b) events with 2 jets. For the data-background samples, plots a) and b) show the number of jets in 1 jet events and in 2 jet events respectively. The Monte Carlo samples are normalised in plot a) to the number of 1 jet events in the data-background sample, and in b) to the number of 2 jet events in the data-background sample. The samples are represented as in figure 2 and the errors in the data-background sample are purely statistical.